Contents lists available at ScienceDirect

Case Studies in Thermal Engineering
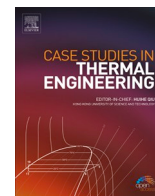
Experimental investigation and thermal analysis of solar air heater having rectangular rib roughness on the absorber plate

Clement A. Komolafe[a,*], Iyiola O. Oluwaleye[b], Omojola Awogbemi[b,c], Christian O. Osueke[a]

[a] *Department of Mechanical Engineering, College of Engineering, Landmark University, P.M.B. 1001, Omu Aran, Nigeria*
[b] *Department of Mechanical Engineering, Faculty of Engineering, Ekiti State University, P.M.B. 5363, Ado Ekiti, Nigeria*
[c] *Discipline of Mechanical Engineering, Howard College Campus, University of KwaZulu-Natal, Durban, 4041, South Africa*

A B S T R A C T

This study presents experimental investigation and thermal analysis of solar air heater having rectangular roughness on the absorber plate. The solar air heater used for the experiment was locally fabricated. The maximum intensity of solar radiation, ambient and solar air heater temperature were $827.87 \, W/m^2$, 33.77 and 112.0 °C respectively during the day time period of 9:00–18:00 h operation. The calculated thermal efficiency value ranged between 14.0 to 56.5%. The simulated minimum and maximum temperature of the solar air heater were 21 and 127 °C respectively, which were in reasonable agreement with experiment result of 20 and 112 °C. Thus, the solar air heater was considered capable of handling processes such as drying of various agricultural products, water heating etc. with temperature control mechanism.

1. Introduction

Importance of energy in our daily life cannot be over-emphasised considering its usefulness in food processing, preservation, lighting, heating, cooking etc. [1,2]. Renewable energy source has become viable alternative means through which dependable energy could be accessed. Harnessing the abundant potentials in the freely given renewable energy sources such as solar energy has become necessary considering the increase in the cost of fossil fuel, rapid depletion of the world's fossil fuel reserves and also the erratic nature of power supplies in developing counties like Nigeria. The simplest and most efficient method to utilise this freely given energy source is to transform solar radiation into thermal energy for heating application using collectors, Sonalkar et al. [3]. Solar energy has been adjudged the most viable and reliable of all other renewable sources in the world because it is clean and abundant, Panwar, [4]. Heating can be done by solar thermal energy using different configurations. There are three types of solar collectors namely: flat plate, evacuated tube, and parabolic trough. Among the three, flat plate collectors are the most common for low temperature applications (323–343 K) [5]. The major areas of application of solar air heater include drying of agricultural products, space heating, curing of industrial products and seasoning of timber, architecture heated, HD desalination [6–9]. Introduction of the rib roughness have been carried out in the cooling channels of gas turbine blades and solar air heater in order to enhance heat transfer, Karwa et al. [10]. Incorporation of different configurations of rib roughness in the form of fine wires on the absorber plate is one of the important and effective design modifications proposed to improve the thermohydraulic performance, Yadav and Bhagoria [11] (Table 1). Several innovative studies have been reported on the design, experimental study and CFD based thermal investigation

---

Nomenclature

A_c	solar collector area of heat transfer, m^2	T_{mp}	weighted mean value of plate temperature, K
C_{pa}	specific heat capacity of air kJ/kgK	U_L	overall heat loss by the collector, W/K
D	hydraulic diameter, mm	u, v, w	velocities in X, Y and Z direction, m/s
f	friction factor	x, y, z	distance along X, Y and Z axis
F_R	collector heat removal factor	X,Y,Z	coordinate axis
G	mass velocity of the air through the duct, m/s		
h	coefficient of heat transfer W/m^2/K	*Greek symbols*	
H	height of the duct, mm		
I	incident insolation, W/m^2	α	thermal diffusivity, m/s
L	Length of the collector, m	ρ	density of air, kg/m^3
$\dot{m}_a$	mass flow rate of air, kg/s	μ	viscosity, kg/ms
Nu	Nusselt number	η	efficiency, %
P	pressure, N/m^2		
δp	pressure drop across the length of the duct N/m^2	*Subscripts*	
Q_g	heat gained by air, W	a	air
Q_u	heat gained by the collector, W	bm	bulk mean
R_e	Reynolds number	c	collector
T	temperature, K	g	gained
T_a	ambient air temperature, K	L	loss
T_{bm}	bulk mean air temperature, K	mp	weighted mean value
T_a	ambient air temperature, K	R	heat removal

Table 1
Thermophysical properties of air, absorber plate(aluminium) and glass [7,14].

Properties	Air	Aluminium	Glass
Density (kg/m^3)	1.1925	2719	2500
Specific heat (J kg^{-1} K^{-1})	1006.2	871	670
Thermal conductivity k (Wm^{-1} K^{-1})	0.0242	202.4	744.3
Viscosity (Nm^{-2})	17894×10^{-05}	–	–
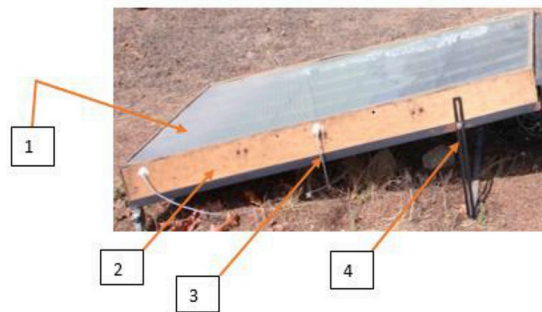
Fig. 1. Pictorial view of the solar air heater. 1. Glass cover 2.Wooden frame 3.Temperature sensor 4. Solar air heater stand.

and analysis of solar air heater having groove or rib roughness ([3,7,10–20]).

In this study, experimental investigation and thermal analysis of a rectangular-sectioned solar air heater having rib roughness incorporated with heat conducting copper chrome pipes were carried out.

2. Materials and methods

2.1. Thermal analysis of the solar air heater

The main concern of the thermal performance of a solar air heater is the heat transfer process within it. The design details in this study had been previously presented in the earlier report of Komolafe and Waheed [21].
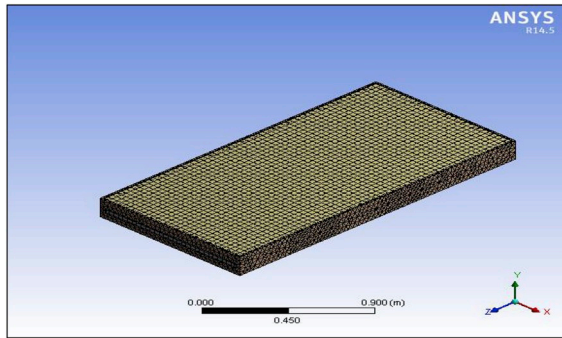
The energy gained by the collector can be calculated using the relation, Gatea, 2010 [22]:
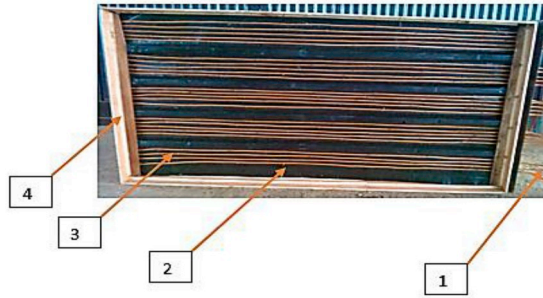
Fig. 2. Arrangement of the heat conducting copper pipes along the ribs. 1. Heated air outlet 2. Black coated aluminium plate 3.Copper pipes 4. Wooden box.
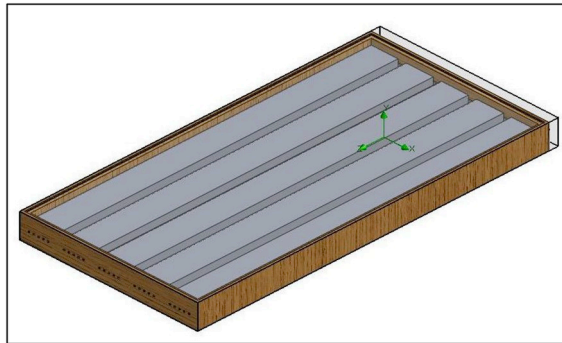
Fig. 3. The 3-D computational domain of the solar air heater.

Fig. 4. The meshed solar air heater.

$$Q_u = \alpha \tau I A_c - U_L A_c (T_c - T_a) \tag{1}$$

where A_c is the solar collector area (m^2), I the incident insolation (W/m^2), U$_L$ the overall heat loss by the collector (W/K), α.the Solar absorptance, τ transmittance of absorber plate, T_c the collector temperature (K), and T_a the ambient air temperature (K).

The heat gained, Sevik, 2013 [23], is given by air:

$$Q_g = \dot{m}_a C_{pa}(T_c - T_a) \tag{2}$$

where $\dot{m}_a$ is mass flow rate of air through the dryer per unit time (kg/s) and C$_{pa}$ the specific heat capacity of air (kJ/kg K)

The coefficient of heat transfer between the air and the heated plate is expressed as Karwa et al. [10]:

$$h = \frac{Q_g}{\{A_c(T_{mp} - T_{bm})\}} \tag{3}$$

where A$_c$ = LB is the collector area of heat transfer, T_{mp} and T_{bm} are weighted mean value of plate temperature and bulk mean air temperature. $\left(\frac{T_o - T_i}{2}\right)$

The Nusselts number and Reynolds number to provide required information on heat transfer quality are given as:
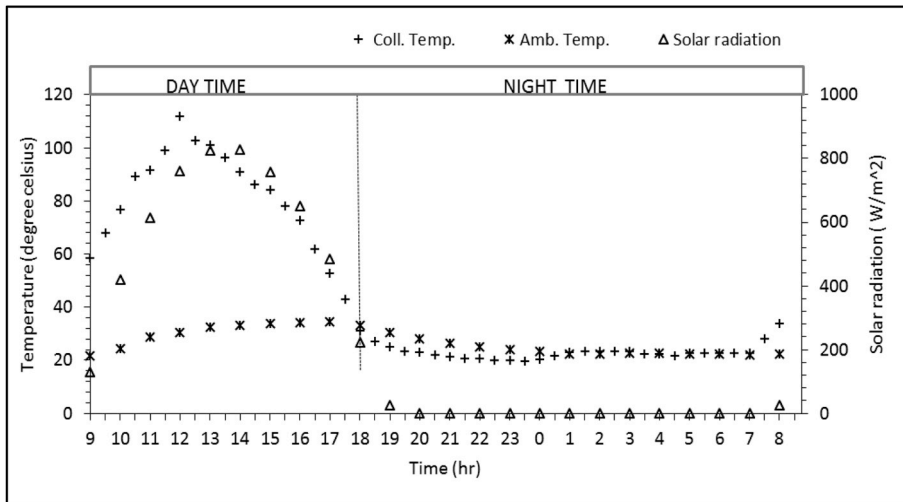
Fig. 5. Variation of solar radiation and temperature of the ambient, and solar collector with time.
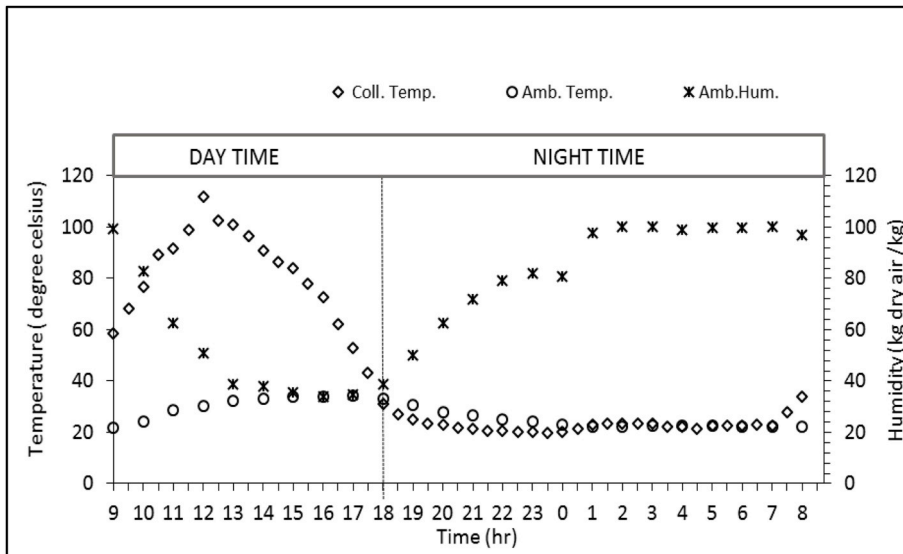

Fig. 6. Variation of humidity and temperature of the ambient, and collector with time.

$$NU = \frac{hD}{k} \tag{4}$$

and

$$Re = \frac{GD}{\gamma} \tag{5}$$

where D = $4BH/\{2(W + H)\}$ is the hydraulic diameter, G = $m/(BH)$ which is the mass velocity of the air through the duct.

The friction factor (f) can be obtained from the measured value of pressure drop δp across the length of the duct using the expression, Karwa et al. [10]:

$$f = \frac{2(\delta p)\rho D}{4LG^2} \tag{6}$$

The collector heat removal factor (F_R) is Alta et al. [24]:

$$F_R = \frac{m_a C_{pa}(T_c - T_a)}{A_c [\alpha\tau I - U_L (T_c - T_a)]} = \frac{Q_g}{Q_u} \tag{7}$$

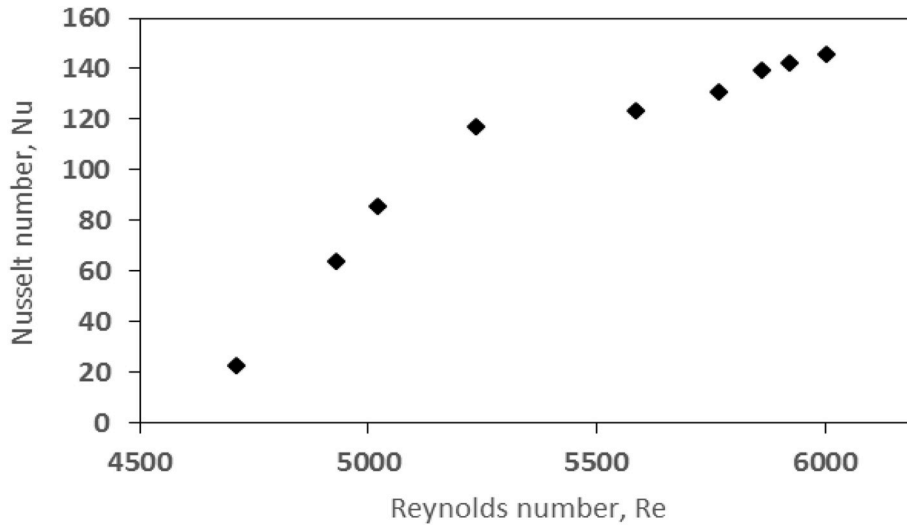The collector efficiency (ɳ) is expressed as Montero et al. [25]:

Fig. 7. Variation of Nusselt number with Reynolds number.
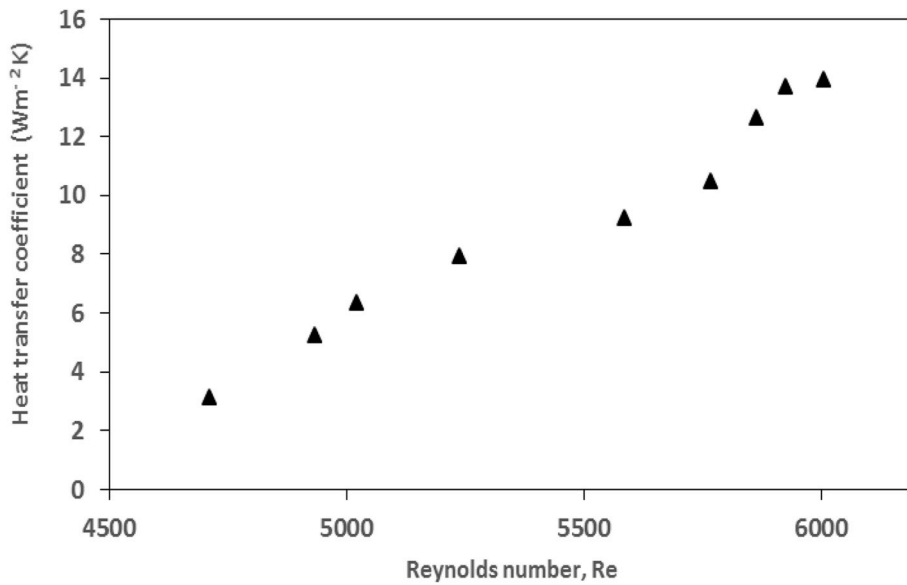
Fig. 8. Plot of heat transfer coefficient against Reynolds number.

$$\eta = \frac{\dot{m}_a C_{pa}(T_c - T_a)}{IA_c} \tag{8}$$

2.2. Computational fluid dynamics approach

Computational fluid dynamics method were used to investigate the interactive motion of large number of individual particles inside the fluid domain, Vyas [14]. It entails numerical solution of the governing equations (non-linear partial differential equation) of continuity, momentum, energy and species. These three dimensional governing equations are summarised as follows.

The mass conservation (i.e. continuity) equation:

$$\frac{\partial u}{\partial x} + \frac{\partial v}{\partial y} + \frac{\partial w}{\partial z} = 0 \tag{9}$$

The momentum equations with constant properties are:

Fig. 9. Variation of friction factor with Reynolds number.

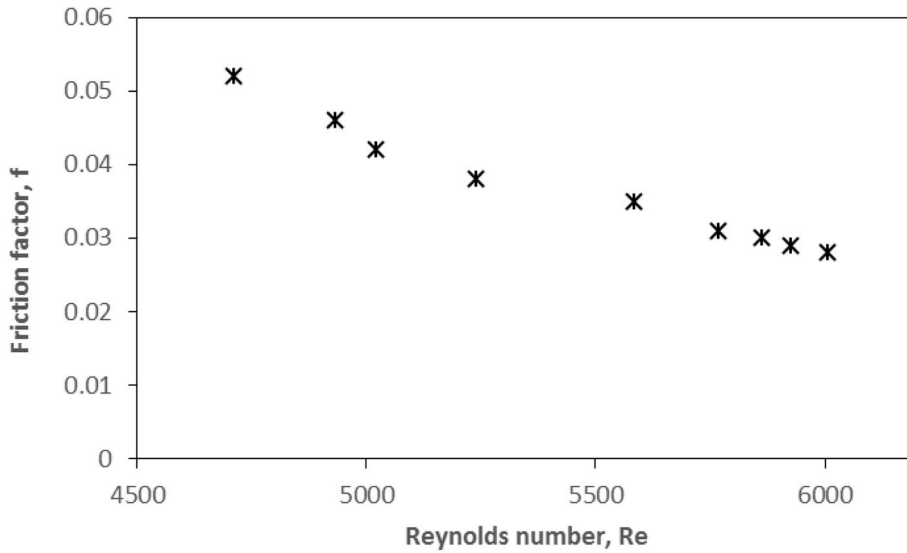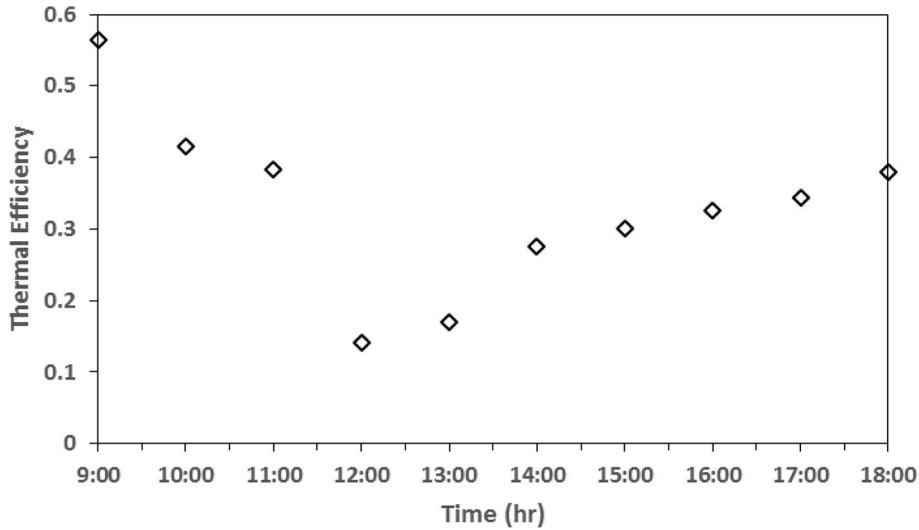Fig. 10. Variation of thermal efficiency with time.

$$\rho\left(U\frac{\partial u}{\partial x} + V\frac{\partial u}{\partial y} + W\frac{\partial u}{\partial z}\right) = -\frac{\partial p}{\partial x} + \mu\left(\frac{\partial^2 u}{\partial x^2} + \frac{\partial^2 u}{\partial y^2} + \frac{\partial^2 u}{\partial z^2}\right)$$

(10)

$$\rho\left(U\frac{\partial v}{\partial x} + V\frac{\partial v}{\partial y} + W\frac{\partial v}{\partial z}\right) = -\frac{\partial p}{\partial y} + \mu\left(\frac{\partial^2 v}{\partial x^2} + \frac{\partial^2 v}{\partial y^2} + \frac{\partial^2 v}{\partial z^2}\right)$$

(11)

$$\rho\left(U\frac{\partial w}{\partial x} + V\frac{\partial w}{\partial y} + W\frac{\partial w}{\partial z}\right) = -\frac{\partial p}{\partial z} + \mu\left(\frac{\partial^2 w}{\partial x^2} + \frac{\partial^2 w}{\partial y^2} + \frac{\partial^2 w}{\partial z^2}\right)$$

(12)

The energy equation with constant properties is

$$\left(U\frac{\partial T}{\partial x} + V\frac{\partial T}{\partial y} + W\frac{\partial T}{\partial z}\right) = -\alpha\left(\frac{\partial^2 T}{\partial x^2} + \frac{\partial^2 T}{\partial y^2} + \frac{\partial^2 T}{\partial z^2}\right)$$

(13)

2.3. Experimental set up

The solar air heater pictorially shown in Fig. 1 consists mainly of top-open wooden box, (2100 x 1100 x 120) mm made from
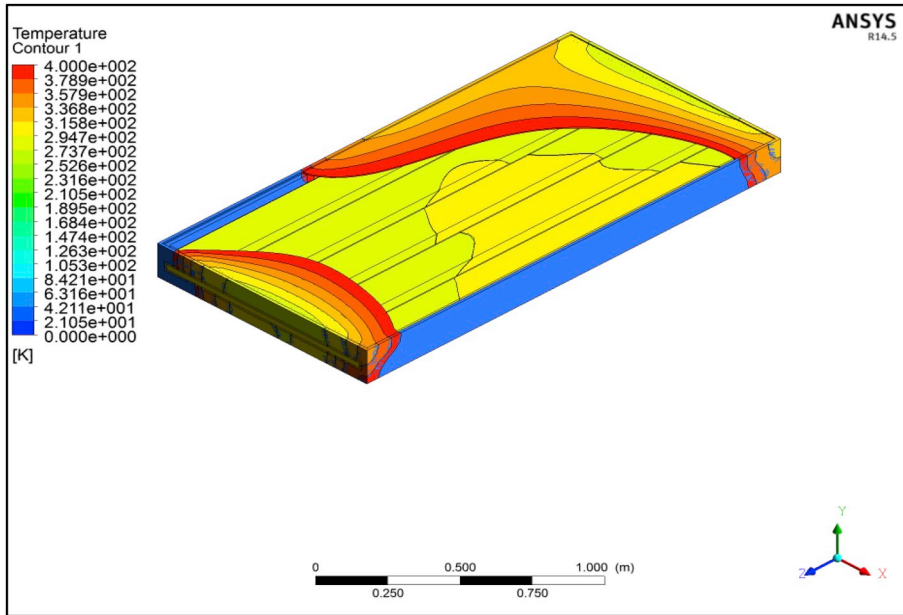
Fig. 11. Temperature profile along the length of the solar air heater.
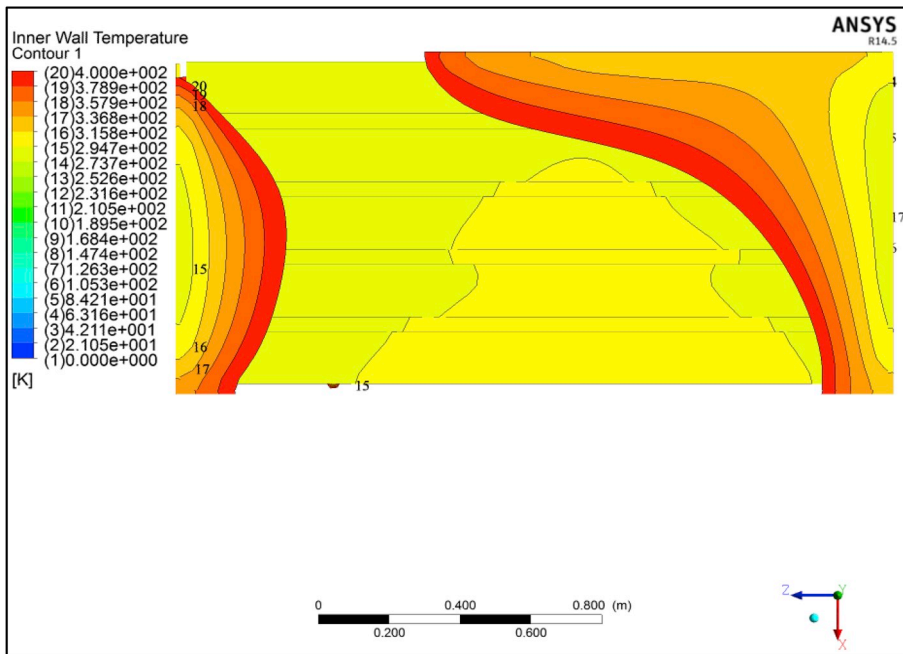
Fig. 12. Inner wall temperature distribution on the absorber plate.

20 mm thick plywood, a 2000 x 1000 mm black painted aluminium sheet having rectangular rib roughness on which air inlet copper pipes were attached as shown in Fig. 2, 50 mm thick rock wool insulation to prevent heat loss in the box and 2000 x 1000 × 4 mm glass. The no load experiments were conducted at the Teaching and Research Farm, Landmark University, Omu Aran, Nigeria on latitude 8° 8′N, longitude 5° 5′ E under natural convection mode from 9:00 h to 18:00 h in order to determine the thermal profile of the solar air heater. Temperature was measured at different locations within the air heater using sensors DS18B20 capable of measuring temperature from −55 to +125 °C (± 0.5 °C accuracy). The sensors were connected to a data logger made up of Atmel ATmega 328P type micro-controller which acts as the brain of the system, SD Card Module for mounting the memory card, a real time clock module for taking note of time and date of the day and a power bank unit which is powered by a 4400 mA H. It was configured and programmed to take readings at interval of thirty minutes (30 min). Data of other vital parameters such as ambient air, relative

humidity and solar radiation etc. were collected from the Campbell Scientific Ltd. manufactured weather station (Data logger Model No: 18728) positioned few metres from the solar air heater.

2.4. Solution technique

The governing equation in their steady, incompressible and three dimensional states were solved after appropriate definition of computational domain, mesh generation, boundary condition using commercial CFD software ANSYS FLUENT 14.5 which is based on finite volume method. The inlet parameters from the experimental studies were used as input data for simulation. The output parameter from the simulation studies were compared with the estimated output parameters for different set of conditions. The overall dimension of the 3-D computational domain (Fig. 3) of the developed solar air heater used for CFD analysis was (2100 x 1100 x 120) mm. Generation of mesh (Fig. 4) without the fluid carrying pipes was carried out by rectangular elements after the definition of the computational domain. The second order upwind scheme was used for discretization of the governing equations, Patankar [26] and Renormalization-group (RNG) k-ε model was engaged to simulate the flow of heat.

3. Results and discussion

Fig. 5 shows the variation of the solar radiation and temperature of the ambient, and collector with time. It is clearly evident from the figure that the two temperatures and the solar radiation increased with time while from the afternoon towards evening, they decreased. The temperature profile follows the same pattern with the solar radiation profile. The measure maximum ambient and collector temperatures were 33.77 and 112.0 °C (385 K) respectively. The solar radiation attained its peak value of 827.87 W/m^2 at 12: 00 h. At 18:00 h, it was observed that the intensity of solar radiation and the temperatures had reduced to 222.55 W/m^2 and 33.0 °C (306 K) respectively. During the night time (between 17:00 h and 8:00 h the following morning), the intensity of solar radiation ranged between 0 and 25.97 W/m^2, and temperatures between 21.5 and 33.8 °C. The maximum collector temperature obtained proved that the solar air heater will be capable of supplying the needed heat for industrial operations such as drying, space heating etc if infiltration losses are minimised while connecting with other units of a system.

In Fig. 6, the relative humidity was plotted over the time. The ambient and collector temperatures were also plotted over time to reveal the effects on the relative humidity. As depicted, the temperatures increased with the time from the morning hour towards noon and decreased towards night time while the relative humidity decreased with time towards noontime and increased towards night time. The minimum and maximum ambient relative humidity values of 33.8 and 99.99% were measured at 16:00 h and 3:00 h (the following morning).

Fig. 7 depicts the plot of Nusselt number with Reynolds number. It can be seen from the figure that the Nusselt number increased from 22.94 to 145.5 with the increase in the Reynolds number from 4711.6 to 6004.63. This may be attributed to the increase in turbulent intensity caused by increase in turbulent kinetic energy and the rate of dissipation, Yadav and Bhagoria [12]. Also, this occurred due to vigorous mixing of primary and secondary flows, reattachment and vortex shedding between the ribs, Sharma and Kalamkar [27]. Similar trends were reported by [11,15,17,18] for solar air heater having square-sectioned transverse rib, transverse rectangular ribs, V-shaped ribs and ribbed triangular duct on the absorber plate respectively.

The plot of heat transfer coefficient against Reynolds number is reported in Fig. 8. Similar to the profile presented in Fig. 7, the heat transfer coefficient increased with the increase in Reynolds number. The maximum heat transfer coefficient and Reynolds number were 13.95 W/m^{2}K and 6004.63 respectively.

The variation of friction factor with Reynolds number is presented in Fig. 9. It can be seen from the two parameters that the friction factor decreased with the increase in Reynolds number. This trend simply interprets that the higher the friction factor the lower the Reynolds number. This may be attributed to suppression of laminar sublayer for fully developed turbulent flow in the duct, Vyas [14].

Fig. 10 shows the variation of the thermal efficiency with time. The values of the thermal efficiency ranged from 14.0 to 56.5% and averagely 33%. This average thermal efficiency obtained in this study was in reasonable agreement with 30.6, 35 and 41% reported by [21,28,29]. The maximum thermal efficiency obtained was higher than 20.3, 29.8 and 35.1% reported by [30] for three configurations of flat plate collector. The mass flow rate varied between 0.032 and 0.056 kg/s. It is evident from the figure that the collector efficiency decreased as the intensity of the solar insolation increases. Also, this is in congruent with the result of study on hybrid solar drying system by [28,29] that at low solar insolation, the thermal efficiency of the collector increased.

Figs. 11 and 12 display the temperature profiles of the solar air heater and inner wall temperature distribution on the absorber plate. It can be observed that the increase in the solar air heater temperature from the inlet to the top was in the range of 21–127 °C (294.7–400 K). The temperature distribution on the absorber plate were almost homogenous. This could be the resultant effect of insulating material which helped to reduce infiltration losses through the walls of the air heater. Comparison between the simulated and experimental (temperature profiles) results revealed that they were in reasonable agreement with each other.

4. Conclusion

A solar air heater with rectangular sectioned rib roughness on the black coated absorber plate was experimentally and numerically investigated for thermal analysis under Omu Aran climate, Nigeria. On the sectioned ribs were heat conducting copper chrome pipes through air enters and exits the heater. Temperature at different locations within the air heater was measured using sensors DS18B20 connected to a data logger. For thermal analysis, the governing equations (Continuity, momentum, energy and

species) were numerically solved for a three-dimensional solar air heater using Finite Volume Method with the aid of ANSYS, a Computational Fluid Dynamic software.

The following were the major results drawn from the study:

1. The maximum intensity of solar radiation, ambient and solar air heater temperature were 827.87 W/m^2, 33.77 and 112.0 °C respectively during the day time period of 9:00–18:00 h operation.
2. The minimum and maximum ambient relative humidity value of 33.8 and 99.99% were measured at 16:00 and 3:00 h morning hour.
3. The calculated thermal efficiency value ranged between 14.0 to 56.5%
4. The simulated minimum and maximum temperature of the solar air heater were 21 and 127 °C respectively, which were in reasonable agreement with experimental result of 20 and 112 °C.

Conflicts of interest

The authors wish to state the there is nothing like conflict of interest in respect to this submission.

References

[1] O. Awogbemi, C.A. Komolafe, Potential for sustainable renewable energy development in Nigeria, Pac. J. Sci. Technol. 12 (1) (2011) 161–169.
[2] O. Awogbemi, I.O. Oluwaleye, C.A. Komolafe, A survey of solar energy utilization for sustainable development in Nigeria, J. Multidiscip. Eng. Sci. Technol. 2 (7) (2015) 1716–1724.
[3] R. Sonalkar, P. Trivedi, CFD Based Performance Analysis of a Roughened Solar Air Heater Duct Having NACA 0030 Airfoils as Artificial Roughness, (2018).
[4] N. Panwar, S. Kaushik, S. Kothari, Role of renewable energy sources in environmental protection: a review, Renew. Sustain. Energy Rev. 15 (3) (2011) 1513–1524 https://doi.org/10.1016/j.rser.2010.11.037.
[5] M.M.A. Khan, N.I. Ibrahim, I.M. Mahbubul, H.M. Ali, R. Saidur, Evaluation of solar collector designs with integrated latent heat thermal energy storage: a review, Sol. Energy 166 (2018) 334–350 https://doi.org/10.1016/j.solener.2018.03.014.
[6] R. Foster, M. Ghassemi, A. Cota, Solar Energy: Renewable Energy and the Environment, CRC Press, Boca Raton, 2010.
[7] S. Chaudhari, M. Makwana, R. Choksi, G. Patel, CFD analysis of solar air heater, Int. J. Eng. Res. Afr. 4 (6) (2014) 47–50.
[8] J.A. Duffie, W.A. Beckman, Solar Engineering of Thermal Processes, John Wiley and Sons, 2013.
[9] G. Cheng, L. Zhang, Numerical simulation of solar air heater with V-groove absorber used in HD desalination, Desalination and Water Treatment 28 (1–3) (2011) 239–246 https://doi.org/10.5004/dwt.2011.1820.
[10] R. Karwa, B. Maheshwari, N. Karwa, Experimental study of heat transfer enhancement in an asymmetrically heated rectangular duct with perforated baffles, Int. Commun. Heat Mass Transf. 32 (1–2) (2005) 275–284, https://doi.org/10.1016/j.icheatmasstransfer.2004.10.002.
[11] A.S. Yadav, J. Bhagoria, Modeling and simulation of turbulent flows through a solar air heater having square-sectioned transverse rib roughness on the absorber plate, Sci. World J. (2013), https://doi.org/10.1080/10407782.2013.846187.
[12] A.S. Yadav, J. Bhagoria, A CFD analysis of a solar air heater having triangular rib roughness on the absorber plate, Int. J. ChemTech Research 5 (2) (2013) 964–971.
[13] P.W. Ingle, A.A. Pawar, B.D. Deshmukh, K.C. Bhosale, CFD analysis of solar flat plate collector, Int. J. Emerg. Technol. Adv. Eng. 3 (4) (2013) 337–342.
[14] A.A. Vyas, D. Shringi, CFD based thermal efficiency analysis of solar air heater with smooth plate and perforated plate, Imp. J. Interdiscip. Res. 3 (2) (2017).
[15] A. Boulemtafes-Boukadoum, A. Benzaoui, CFD based analysis of heat transfer enhancement in solar air heater provided with transverse rectangular ribs, Energy Procedia 50 (2014) 761–772 https://doi.org/10.1016/j.egypro.2014.06.094.
[16] W. Jedsadaratanachai, A. Boonloi, Thermal performance improvement in a square channel heat exchanger with various parameters of v-wavy plates, Frontiers in Heat and Mass Transfer (FHMT) (2018) 12, https://doi.org/10.5098/hmt.12.1.
[17] D. Jin, M. Zhang, P. Wang, S. Xu, Numerical investigation of heat transfer and fluid flow in a solar air heater duct with multi V-shaped ribs on the absorber plate, Energy 89 (2015) 178–190 https://doi.org/10.1016/j.energy.2015.07.069.
[18] R. Kumar, V. Goel, A. Kumar, S. Khurana, Numerical investigation of heat transfer and friction factor in ribbed triangular duct solar air heater using Computational fluid dynamics (CFD), J. Mech. Sci. Technol. 32 (1) (2018) 399–404, https://doi.org/10.1007/s12206-017-1240-8.
[19] H. Mzad, K. Bey, R. Khelif, Investigative study of the thermal performance of a trial solar air heater, Case Studies in Thermal Engineering 13 (2019) 100373 https://doi.org/10.1016/j.csite.2018.100373.
[20] I. Zulkifle, A.H.A. Alwaeli, M.H. Ruslan, Z. Ibarahim, Numerical investigation of V-groove air-collector performance with changing cover in Bangi, Malaysia, Case studies in thermal engineering 12 (2018) 587–599 https://doi.org/10.1016/j.csite.2018.07.012.
[21] C.A. Komolafe, M.A. Waheed, Design and fabrication of a forced convection solar dryer integrated with heat storage materials, Annale de Chimie-Science des Materiaux 42 (1) (2018) 215–223, https://doi.org/10.3166/acsm.42.23-39.
[22] A.A. Gatea, Design, construction and performance evaluation of solar maize dryer, J. Agric. Biotechnol. Sustain. Dev. 2 (3) (2010) 39–46.
[23] S. Şevik, Design, experimental investigation and analysis of a solar drying system, Energy Convers. Manag. 68 (2013) 227–234 https://doi.org/10.1016/j.enconman.2013.01.013.
[24] D. Alta, E. Bilgili, C. Ertekin, O. Yaldiz, Experimental investigation of three different solar air heaters: energy and exergy analyses, Appl. Energy 87 (10) (2010) 2953–2973 https://doi.org/10.1016/j.apenergy.2010.04.016.
[25] I. Montero, J. Blanco, T. Miranda, S. Rojas, Design, construction and performance testing of a solar dryer for agroindustrial by-products, Energy Convers. Manag. 51 (7) (2010) 1510–1521 https://doi.org/10.1016/j.enconman.2010.02.009.
[26] S.K. Patankar, Numerical Heat Transfer and Uid Ow, Hemisphere, New York, 1980.
[27] S.K. Sharma, V. Kalamkar, Numerical investigation of convective heat transfer and friction in solar air heater with thin ribs, Comput. Model. Eng. Sci 114 (3) (2018) 295–319, https://doi.org/10.3970/cmes.2018.114.295.
[28] A. Fudholi, K. Sopian, M.Y. Othman, M.H. Ruslan, Energy and exergy analyses of solar drying system of red seaweed, Energy Build. 68 (2014) 121–129 https://doi.org/10.1016/j.enbuild.2013.07.072.
[29] A. Fudholi, R. Yendra, D.F. Basri, M.H. Ruslan, Energy and exergy analysis of hybrid solar drying system, Contemp Eng Sci 9 (5) (2016) 215–223 https://doi.org/10.12988/ces.2016.512323.
[30] K.B. Koua, E.P.M. Koffi, P. Gbaha, Thermal performance amelioration of flat plate solar collector of an indirect dryer, Mathematical Modelling of Engineering Problems 5 (2018) 341–347 https://doi.org/10.18280/mmep.050410.